Atmospheric Environment 55 (2012) 190–200

Contents lists available at SciVerse ScienceDirect

Atmospheric Environment

journal homepage: www.elsevier.com/locate/atmosenv

Aerosol optical properties at Pasadena, CA during CalNex 2010

Jonathan E. Thompson [a,*], Patrick L. Hayes [b], Jose L. Jimenez [b], Kouji Adachi [c,1], Xiaolu Zhang [d], Jiumeng Liu [d], Rodney J. Weber [d], Peter R. Buseck [c]

[a] Department of Chemistry & Biochemistry, MS 1061, Texas Tech University, Lubbock, TX 79409, USA
[b] Cooperative Institute for Research in Environmental Sciences and Department of Chemistry & Biochemistry, University of Colorado, Boulder, USA
[c] School of Earth and Space Exploration and Department of Chemistry and Biochemistry, Arizona State University, Tempe, AZ, USA
[d] School of Earth and Atmospheric Science, Georgia Institute of Technology, 311 Ferst Drive, Atlanta, GA, USA

ARTICLE INFO

Article history:
Received 6 January 2012
Received in revised form
28 February 2012
Accepted 2 March 2012

Keywords:
Aerosol optics
Single scatter albedo
Scattering coefficient
Extinction coefficient
Absorption coefficient
Mass absorption cross section
Mass scatter efficiency
Direct climate forcing
CalNex
Albedometer
Brown carbon
WSOC
Absorption enhancement

ABSTRACT

Aerosol optical properties measured at the Pasadena, CA site during the CalNex field campaign in May–June 2010 are summarized. Average measurements of $PM_{2.5}$ aerosol extinction, scattering, absorption coefficients, and single scattering albedo (b_{ext}, b_{scat}, b_{abs} and SSA) at $\lambda = 532$ nm were 62 Mm^{-1}, 58 Mm^{-1}, 4 Mm^{-1}, and 0.92, respectively. The aerosol optical densities were 5 times lower than during the SCAQS study in 1987, highlighting major progress in PM control in the Los Angeles area in the last two decades. The period May 30–June 8 2010 was characterized by exceptionally high aerosol loading (b_{ext} up to 250 Mm^{-1}). During this period, b_{ext}, b_{scat}, and SSA tended to peak during the mid-morning. Correlation of $PM_{2.5}$ b_{ext}, b_{scat} with mass concentration data yielded mass scattering and mass extinction coefficients of 3.5–5.1 $m^2\ g^{-1}$ for 532 nm. Aerosol b_{abs} were compared directly to mass concentration of elemental carbon (EC) yielding a campaign average mass absorption cross section (M.A.C.) of 5.7 ± 1.8 $m^2\ g^{-1}$. TEM analysis of particles suggests soot was often internally mixed or adhering to sulfate and/or organics. Total non-refractory PM_1 mass was a good quantitative indicator of coated soot fraction. Alteration of M.A.C. with mixing/coating state was not detected, however, increases in M.A.C. were linked to the presence of light absorbing, water-soluble organic carbon (WSOC) suggesting a possible role of this material invisible light absorption in the LA basin.

1. Introduction

Atmospheric particles (aerosols) of nm–μm dimensions that are often present at concentrations of less than 40 μg m^{-3} of air can have profound effects on air quality, climate, and human health (I.P.C.C., 2007; Bell et al., 2010; Atkinson et al., 2010). Developing a better understanding of the chemical and physical processes involved in the production, transformation, and fate of atmospheric particulate matter is important to constrain the aerosols effect on climate. Atmospheric aerosols scatter and absorb sunlight in the atmosphere and thereby decrease solar irradiance at Earth's surface and alter tropospheric actinic flux and photochemistry. To quantify these optical effects, aerosol related scattering can be described by the scattering coefficient (b_{scat}). Similarly, aerosol-related absorption can be quantified by absorption coefficient (b_{abs}). Both b_{scat} and b_{abs} have units of inverse distance (often Mm^{-1} units used). The extinction coefficient (b_{ext}) is the total light attenuation resulting from the sum of both optical effects. Light attenuation can then be described through a simple Beer–Lambert law approach:

$$b_{ext} = b_{scat} + b_{abs} \quad (1)$$

$$I(z) = I_0 e^{-1_{ext} z} \quad (2)$$

where z is the path length through the medium.

While both scattering and absorption can attenuate light, the photochemical and climate implications of these optical effects differ. For instance, pure scattering leads to a cooling effect on climate. On the other hand, absorption by aerosols can increase solar heating aloft and potentially lead to a climate warming effect. Therefore, apportioning extinction into the separate effects of scattering and absorption is key for understanding the climate effects of aerosols. A useful variable to describe the relative effects

* Corresponding author. Tel.: +1 806 742 3210; fax: +1 806 742 1289.
E-mail address: jon.thompson@ttu.edu (J.E. Thompson).
[1] Current address: Meteorological Research Institute, Atmospheric Environment and Applied Meteorology Research Department, Tsukuba, Ibaraki, Japan.

1352-2310/$ – see front matter © 2012 Elsevier Ltd. All rights reserved.
doi:10.1016/j.atmosenv.2012.03.011

of scattering vs. absorption is the single scattering albedo (SSA). SSA is a dimensionless number between 0 and 1 and is defined as the ratio of the scattering and extinction coefficients:

$$SSA = \frac{b_{scat}}{b_{ext}} \quad (3)$$

Non-absorbing aerosols have SSA = 1, while those that absorb are associated with a lower value. Accurate and precise measurements of SSA are important since small changes in its value can significantly influence the net radiative forcing of aerosols (Haywood and Shine, 1995; Haywood and Boucher, 2000).

It is also convenient to link the optical properties of aerosols to mass concentrations through parameters called mass extinction (m_{ext}), mass scattering (m_{scat}), and mass absorption (m_{abs}) efficiencies or cross sections (all with units of $m^2\ g^{-1}$). These values express an optical effect per unit mass and, can be thought of as the slope of the best-fit line linking each optical effect with the mass concentration of the aerosol. For absorption, it has historically been believed that the elemental carbon fraction (EC, here assumed to be equivalent to soot) is primarily responsible for absorption of visible light. So often the focus lies solely on the mass absorption cross section of EC – here termed M.A.C. However, more recent research suggests organic compounds in aerosols (brown carbon) may also contribute to light absorption, and if not accounted for can bias determination of M.A.C. to falsely high values (Andreae and Gelencsér, 2006).

The CalNex 2010 field campaign performed research at the nexus of climate change and air quality in California, USA (http://www.esrl.noaa.gov/csd/calnex/, http://cires.colorado.edu/jimenez-group/wiki/index.php/CalNex-LA, http://www.arb.ca.gov/research/calnex2010/calnex2010.htm.). The campaign measurement strategy featured simultaneous measurements at several ground sites, and on-board instrumented aircraft and ships. The Pasadena ground site featured an impressive array of >40 particle and gas phase measurements to investigate trends for a continuous one month sampling period (May 15–June 15 2010). In this paper, we highlight $PM_{2.5}$ optical properties of aerosols observed at Pasadena during CalNex. This includes:

(1) Presentation of a statistical treatment of optical data and diurnal patterns for the period of study, and comparison with past values in the Los Angeles basin and current values in developing world megacities. Results suggest substantial improvements in regional air quality.
(2) Correlation analysis of optical and mass concentration data that report aerosol mass scattering and extinction coefficients (m_{scat} and m_{ext}; $m^2\ g^{-1}$). This data allows reconstruction of aerosol optical effects from ground based measurements of mass concentration.
(3) A comparison of b_{abs} with EC mass concentration to determine campaign average M.A.C. Results are similar to values postulated for fresh soot. However, the soot M.A.C. measurement is influenced by water-soluble brown carbon absorption.
(4) A transmission electron microscopy (TEM) study that indicates soot particles often exist internally mixed with organics and sulfate – and the resulting particles exhibit complex morphologies. Soot coating fractions obtained through TEM increase with AMS non-refractory (NR) PM_1 mass concentrations.

2. Experimental

2.1. Sampling site, meteorology & period

The sampling site was located at 34.140582 N, −118.122455 (+34° 8′ 26.10″, −118° 7′ 20.84) in Pasadena, CA on the campus of the California Institute of Technology. The measurement period was from May 15, 2010 0:00 (local) to June 16 0:00 (local). A typical daily temperature cycle during the measurement period featured temperatures of 10–15 °C at night rising to approx. 25 °C during the day. Ambient relative humidity (RH) often approached 100% overnight and fell to ≈50–60% by late afternoon local time. The prevailing winds were often from the southwest (often near 200°) and usually light (<4 m s^{-1}) with a strong diurnal cycle. Sunrise was typically approximately 5:30 AM and sunset approximately 8:00 PM local time during the sampling period. Wind roses, temperature, and relative humidity data has been presented in Supplementary material figs. S-1 and S-2 available online.

2.2. Aerosol optical measurements from aerosol Albedometer

The aerosol albedometer has been described previously (Thompson et al., 2008; Dial et al., 2010) so only an overview is provided here. Aerosol extinction, b_{ext} is measured through ring-down spectroscopy while b_{scat} is measured simultaneously by integrating sphere nephelometry. The scattering measurement was calibrated through use of a span gas (SUVA, R-134a) with a Rayleigh multiplier of 7.25 times air (Zadoo and Thompson, 2011). The SSA can then be computed directly after applying a correction scheme for angular truncation (Qian et al., submitted for publication; Qian, 2011) and b_{abs} was determined by the difference between extinction and scattering:

$$b_{abs} = b_{ext} - b_{scat} \quad (4)$$

The correction factors were generated through use of size-distribution data obtained using a scanning mobility particle sizer (SMPS) at the site and empirical observations of albedometer response as a function of particle size. The correction factors used are presented in Supplementary material fig. S-4 available online.

Albedometer measurements were made from May 15 to June 10. Instrument calibration and checks were performed periodically by the instrument operator (often near 8:00 AM and 5:00 PM local time). Prior to optical measurement, the ambient aerosol was sampled through a $PM_{2.5}$ cyclone (BGI Inc.) before passing through an approx. 6 m of 1.2 cm i.d copper tubing. The precision for measurement on aerosols (5 min averaging time) is estimated to be 3 Mm^{-1} on both scatter and extinction channels yielding a propagated precision on the absorption channel of 4.2 Mm^{-1}. The optical cell pressure was consistently 0.96–0.97 atm. Cell temperature varied between 281 and 309 K and sample relative humidity (RH) for the data reported was <50%. A diffusion dryer (TSI 3062) was used to dry the sample. Optical properties or diameters of aerosols usually do not change significantly below 50% RH (Yan et al., 2009; Hand et al., 2010; Malm et al., 2005; McMurry and Stolzenburg, 1989).

2.3. Aerosol mass spectrometer

The concentrations of submicron non-refractory ($NR\text{-}PM_1$) organic and inorganic (nitrate, sulfate, ammonium) aerosol particles were measured using a high resolution time-of-flight aerosol mass spectrometer (DeCarlo et al., 2006) (HR-ToF-AMS, Aerodyne Research Inc.). The HR-ToF-AMS sampled from an inlet equipped with a $PM_{2.5}$ cyclone located 2 m above the roof of the container housing the instrument. The ambient air passed through a 6.8 m insulated copper inlet line and a silica (5/15 00:00–6/9 14:00 PDT) or Nafion (6/9 14:00–6/16 00:00 PDT) drier prior to sampling by the HR-ToF-AMS. The resulting data was averaged over 2.5 min intervals. The ion paths through the time-of-flight chamber were alternated between "V" and "W" mode every 150 s, and the reported concentrations from the HR-ToF-AMS correspond to V-

mode acquisition periods only. All data were analyzed using standard HR-ToF-AMS software (SQUIRREL v1.51 and PIKA v1.10) within Igor Pro 6.2.1 (Wave Metrics, Lake Oswego, OR) (Sueper, 2011).

2.4. TEM analysis

For the TEM analysis, aerosol particles were collected with 3-stage impactor samplers (MPS-3, California Measurements, Inc.). We used TEM grids from the smallest impactor stage, with 50% lower and upper cut-off aerodynamic diameters at 0.05 and 0.3 μm, respectively. TEM images were obtained using a CM 200 (Philips Corp.) at an accelerating voltage of 200 kV. In total, 465 TEM samples were collected during the CalNex campaign. For most days, TEM samples were collected at 1-h intervals from 7:00 to 22:00 (local time) and 3-h intervals for the rest of the day. Sampling times were <30 min, and most were <10 min. The sampling time for the TEM samples were adjusted to collect adequate particle number concentrations on the substrates, and only a small fraction of particles may coalesce with each other on the TEM grids when collected.

TEM images were obtained from ~20 areas on each TEM grid, and each image included ~30 aerosol particles. We chose representative TEM images for each sample to determine the fraction of coated soot particles. The fractions were estimated from TEM images and have large uncertainties because of limited particle numbers, shadowing by other particles, and evaporation of semi-volatile materials within the TEM chamber. We grouped coatings on soot into five bins: 1) none observed, 2) light, 3) moderate, 4) heavy, and 5) complete. Here light, moderate, and heavy are approximately equivalent to 1–25%, 26–74%, and 75–99%, respectively, of volume fractions of coated soot relative to all soot in a sample. Groups 4) and 5) generally mean that the soot is best described as embedded (Adachi et al., 2010).

2.5. EC/OC, PILS and WSOC absorption measurements

$PM_{2.5}$ organic and elemental carbon (OC and EC) were measured semi-continuously with a Sunset Labs EC/OC analyzer (Model 3F, Forest Grove, OR) following NIOSH method 5040 (NIOSH, 1996; Birch, 1998). The instrument was operated to collect sample on an internal quartz filter from the beginning of each hour for 45 min, followed by a 15-min analysis period. An attempt was made to limit positive artifacts by denuding ambient sample air of volatile gases via an inline parallel plate carbon denuder (Eatough et al., 1993). The same denuder, without regeneration was used throughout the 1-month CalNex campaign. Blank measurements were systematically made throughout the study period by placing a Teflon filter on the $PM_{2.5}$ cyclone inlet. A linear change in blank concentrations were assumed between consecutive blank measurements and subtracted from the ambient data. OC blanks ranged from 1.3 to 2.6 μg C m^{-3} and EC blanks 0 to 0.03 μg C m^{-3}. Uncertainty of the EC analysis is estimated to be 28%. A lower limit of quantitation for the EC/OC analyzer of 0.5 μg C m^{-3} was used for the M.A.C. analysis in this study.

One Particle-Into-Liquid Sampler (PILS) was coupled to an ion chromatograph for measurements of soluble anions following methods similar to those described elsewhere (Orsini et al., 2003), and a second PILS was coupled with a Liquid Wave guide Capillary Cell (LWCC) and a Total Organic Carbon (TOC) analyzer for continuous measurements of light absorption and carbon mass content of ambient fine particle ($PM_{2.5}$) liquid extracts (Sullivan et al., 2004; Hecobian et al., 2010). Light absorption spectra between wavelengths of 200 and 800 nm were measured with a UV/Vis spectrophotometer. Three dynamic blank measurements were performed daily (3:00, 10:00 and 19:00), each for 20 min to account for any sampling artifacts throughout the study. The overall measurement uncertainty is estimated at 8% and the limit of detection (LOD) for ions and WSOC is 0.02 μg $m^{-3}$and 0.1 μg C m^{-3}, respectively. In this study, light absorption coefficients averaged between 360 and 370 nm (called [WSOC Abs.] with units of m^{-1}) are used as a measure of water soluble brown carbon fraction of $PM_{2.5}$. Ångstrom exponent of the absorption data is determined from the linear regression fit of light absorption coefficients and wavelengths ranging between 300 and 550 nm on natural log-log plots. $PM_{2.5}$ soluble ion data were based on a 20 min cycle and the WSOC optical absorption data were reported on a 10 min cycle.

2.6. Particle mass concentrations and size distributions

The mass concentration of aerosol components was measured in three different ways. First, PM_1 mass concentration (μg m^{-3}) was reconstructed as the sum of organics, nitrate, sulfate, ammonium, and EC. For this approach, the AMS data stream provided all mass concentrations except EC. Reconstructed AMS PM_1 mass concentrations agreed well with those estimated from scanning mobility particle sizer (SMPS) measurements ($R^2 = 0.85$, with a slope of 1.03 for the linear fit by orthogonal-distance regression). For the period between 6/4 00:00 and 6/7 00:00 a shift in the particle size distribution to larger particles is observed, which is not optimal for AMS measurements given the reduction in particle transmission efficiency near 1 micron diameters for the AMS aerodynamic lens under the conditions of this study. Consequently, data from these periods were not used for the analysis of the mass scattering coefficient.

At the site, located ~40 km from the ocean, sea salt can be a significant fraction of the overall $PM_{2.5}$ mass and hence $PM_{2.5}$ optical properties. In addition to soot, the AMS does not measure other refractory aerosol components such as salts, mineral dust, or metals. As such, a second approach was to use anion data (chloride, sulfate, nitrate) from a particle into liquid sampler (PILS) to compute aerosol mass concentrations. PILS cation measurements were not made throughout this study so the AMS ammonium and organic data was summed with the PILS anion mass concentration and EC for this approach.

The third approach for determining aerosol mass concentration is to use hourly $PM_{2.5}$ data from the β-attenuation monitor (BAM) located at the Burbank California Air Resources Board (CARB) site (site 70,069, Latitude: 34°10′33″ Longitude: 118°19′1″). The Pasadena CalNex site is located approximately 18 km from the Burbank site, however, both sites are located within the LA basin and analysis of 48 h integrated $PM_{2.5}$ gravimetric data for the two sites during 2010 reveals good correlation ($R^2 = 0.8$) between the sites. Additionally, the slope of a best-fit line correlating the sites was 1.04, indicating the Burbank site exhibits only slightly higher mass concentrations on average. Nonetheless, the fairly good agreement between PM loading at the two sites helps to validate comparisons between $PM_{2.5}$ optical properties measured in Pasadena and the mass concentrations from the Burbank monitoring station. Data was averaged to a 1 h time base for all data streams for subsequent analysis.

A scanning mobility particle sizer (SMPS, Model 3936, TSI Inc.) measured ambient number distributions between 7 and 690 nm. The SMPS was operated at a sampling frequency of 5 min and used the same sample inlet as described for HR-ToF-AMS, except that the aerosol flow passed through an additional 0.8 m of copper inlet line. The light scattering was calculated using Mie Theory and the dN/dlogDp data from the SMPS measurements. For these calculations a wavelength of 532 nm was used, as well as a constant index of refraction of 1.53, which corresponds to dry ammonium sulfate. Organics present in aerosols also often have refractive indices near 1.5 (Redmond et al., 2010; Redmond and Thompson, 2011) and the refractive index of ammonium nitrate is 1.55.

3. Results & discussion

3.1. Campaign averages

Fig. 1 shows the time series of observed optical properties and mass concentrations for the measurement period. The campaign average values and standard deviations of b_{ext}, b_{scat}, b_{abs} and SSA were 62 ± 44 Mm^{-1}, 58 ± 43 Mm^{-1}, 3.8 ± 3.4 Mm^{-1}, and 0.92 ± 0.08, respectively. Highest aerosol loading occurred during the first few days of the campaign and during the first week of June. The period of 22–31 May was characterized by relatively low aerosol mass loadings. Fig. 2 illustrates histograms for the optical parameters measured with the albedometer. Despite the lower mean of 0.92 for SSA, the most frequently observed SSA was ≈0.96.

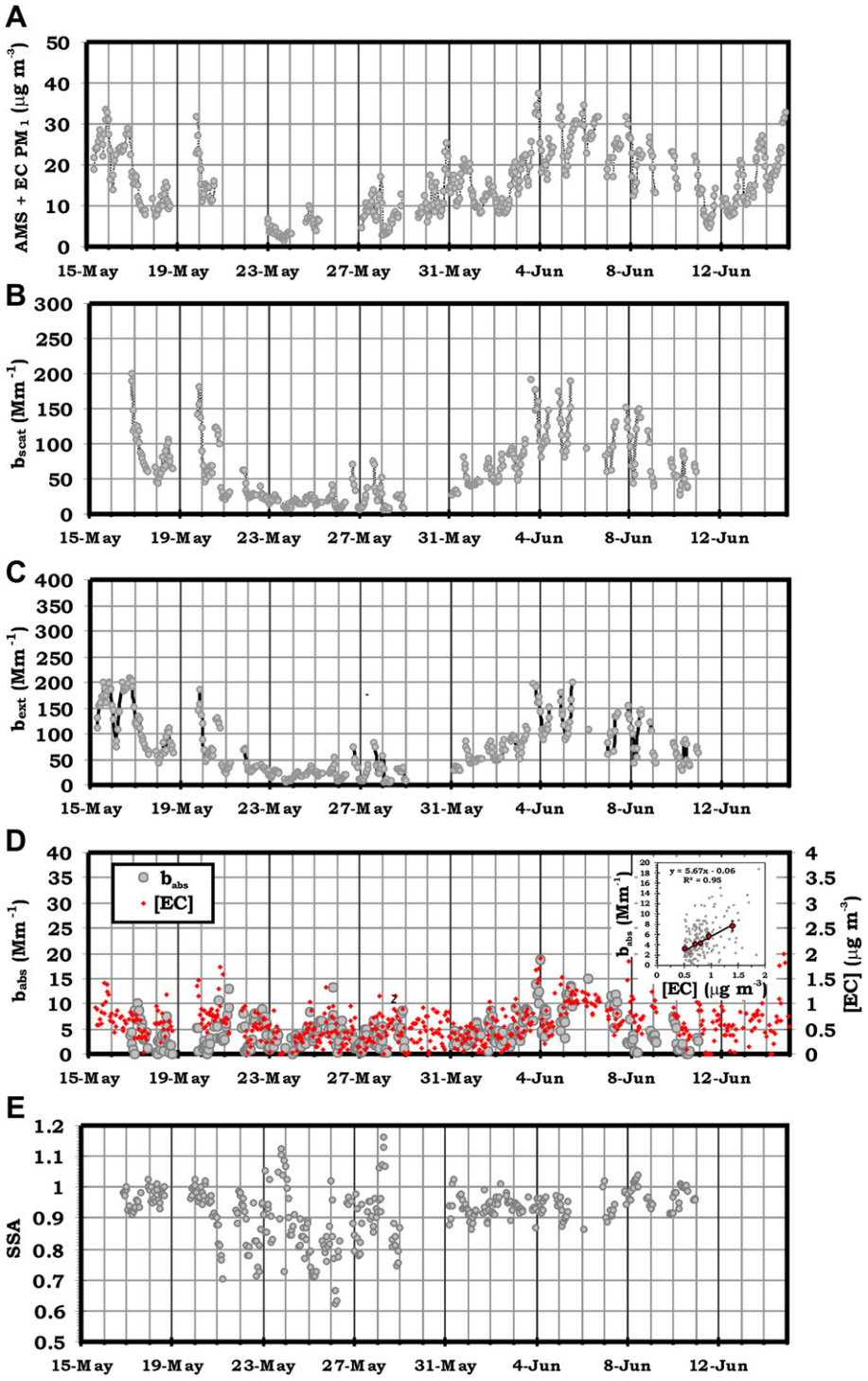

Fig. 1. Time series of (A) AMS + EC PM_1 mass concentration, (B) aerosol scattering coefficient (b_{scat}), (C) aerosol extinction coefficient (b_{ext}) (D) aerosol absorption coefficient (b_{abs}) and elemental carbon (EC) concentration, and (E) single scattering albedo (SSA) observed at Pasadena, CA during May–June 2010. All times and dates are UTC. The inset to (D) illustrates correlation of b_{abs} and EC mass concentration. The large variability in SSA observed at the end of May is a consequence of very low aerosol loadings.

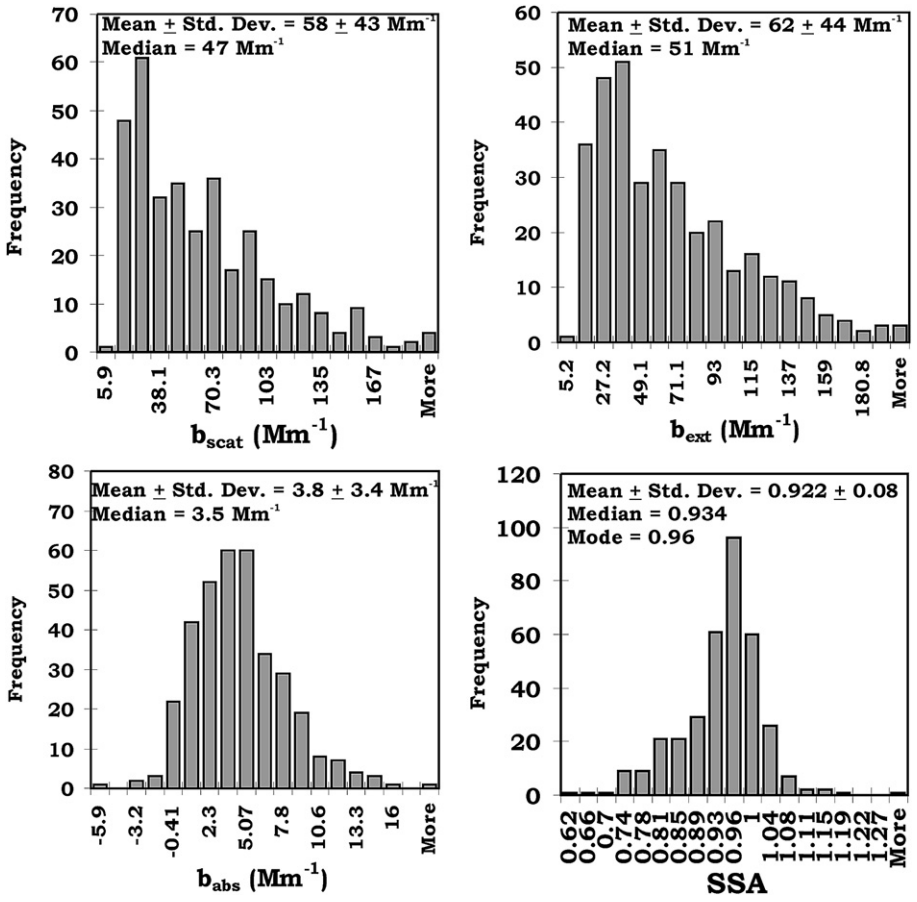

Fig. 2. Histograms summarizing $PM_{2.5}$ aerosol optical properties observed during CalNex 2010 at Pasadena, CA via the aerosol albedometer. b_{scat} – aerosol scattering coefficient, b_{ext} – aerosol extinction coefficient, b_{abs} – aerosol absorption coefficient, SSA – aerosol single scattering albedo.

Albedometer b_{ext} values correlate very well with extinction measurements made with the Aerodyne CAPS instrument at the site ($R^2 = 0.99$).

To determine whether aerosol loadings encountered during CalNex are representative of the location, we examined $PM_{2.5}$ mass concentration data collected at a site in Pasadena (approx. 1 km from our sampling site) by the South Coast Air Quality Management District (K. Durkee, unpublished data, 2011). The annual mean gravimetric $PM_{2.5}$ mass concentration reported for Pasadena in 2010 is very close (4% higher) to the average reported May–June 2010 suggesting aerosol loadings encountered during CalNex are typical of the location.

Comparing the CalNex optical measurements with the historical record is also of interest. In the summer of 1987, Adams et al. (1990) made measurements of aerosol scattering and absorption in the vicinity of Los Angeles (Claremont McKenna College, Claremont, CA) using a nephelometer ($\lambda = 500$ nm) and photoacoustic spectrometer ($\lambda = 514$ nm) as part of the Southern California Air Quality Study (SCAQS). These authors reported a range of b_{abs} of 7–90 Mm^{-1} with an average of 34 Mm^{-1}. In addition, the average concentration of EC reported in the 1987 study was 3.3 $\mu g\ m^{-3}$ Adams et al. (1990) also reported mean scattering and extinction coefficients on the order of 297 and 330 Mm^{-1}, respectively. However, the aerosol sample was apparently not dried in that study and the sample was likely cooled during sampling by an air conditioner (e.g. possible RH effects). Nevertheless, the CalNex 2010 results suggests the Los Angeles aerosol may have experienced a major reduction due to air pollution control measures, becoming about five times less optically dense, and nearly ten fold less light absorbing between 1987 and 2010, consistent with air quality monitoring trends (Croes, 2011; CARB, 2011). Adams et al. (1990) report an average single scattering albedo of 0.89 (co-albedo of 0.11) which is slightly lower than our value.

It is instructive to put these CalNex results in the context of values measured for other urban centers. The optical coefficients observed at Pasadena were about one half of those reported during the MILAGRO campaign in Mexico City (Paredes-Miranda et al., 2009; Marley et al., 2009) consistent with twice as large fine PM concentrations at that location (Aiken et al., 2009). Levels of scattering and extinction near Los Angeles during CalNex are also significantly lower than the averages reported by Garland et al. (2008) for a site downwind of Guangzhou, China, where mean scattering coefficients of 150 Mm^{-1} occurred over a 1 month sampling period during June 2006. The most striking difference between the CalNex data and those for Mexico City and Guangzhou is the mean aerosol absorption coefficient, indicated by the albedometer instrument for Los Angeles was 3.8 ± 3.4 Mm^{-1} (mean ± std. dev. of data). This is significantly less than the mean values reported for both MILAGRO($\approx$30 Mm^{-1}) and downwind of Guangzhou (34 Mm^{-1}). The large difference appears to result from much higher loading of absorbing aerosol components in the developing world megacities compared to the Los Angeles basin. Molina et al. (2010) report average $PM_{2.5}$ EC for the Mexico City sampling sites of 2–4 $\mu g\ m^{-3}$ which about five times that observed at the CalNex LA site during the sampling period ($\approx$0.6–0.7 $\mu g\ m^{-3}$). Also, the campaign average SSA for this CalNex

data set is 0.92 ± 0.08 compared to a mean of 0.82 ± 0.07 for Guangzhou and an SSA between 0.7 and 0.8 for Mexico City. These results indicate the Los Angeles aerosol is much less light absorbing than in Mexico City and Guangzhou.

3.2. Diurnal trends from May 31–June 8

Fig. 3 illustrates diurnal average trends for (A) NR-PM_1 + EC mass concentration, (B) extinction, (C) scattering and SSA, (D) EC mass concentration, (E) WSOC absorption at $\lambda = 365$ nm, and (F) absorption coefficients for 31 May 2010–8 June 2010, when higher aerosol concentrations were present. Plots 3B and 3C also include diurnal trends reconstructed from Mie theory and observed particle size distributions (see Supplementary material S-3). All measurements except SSA and [EC] were normalized to the daily mean value for comparison. Both scattering and extinction coefficient peaked in the mid-morning hours before decreasing during the afternoon. This is earlier than the peak in the PM_1 data, which occurred in the afternoon. The difference is likely due to the higher relative fraction of larger particles (with a higher mass scattering efficiency) in the morning hours, compared with smaller particles in the afternoons (see Supplementary material S-3). A Mie scattering calculation using size distribution data from an SMPS was able to quantitatively explain this difference. The SSA peaked during the morning when larger non-absorbing particles (nitrates) were present. Aerosol b_{abs} reached a maximum near noon local time. Both EC and WSOC absorption reached highest levels during mid-day, with EC peaking a few hours prior to WSOC (Zhang et al., 2011). This is consistent with the b_{abs} data. Considering the albedo trace in Fig. 3C, SSA tended to reach a minimum around 8:00 PM. The SSA seemed to slowly increase overnight before reaching a maximum during times of peak scattering/extinction during the mid-morning hours. SSA dropped rapidly during the times EC and WSOC absorption increased before increasing slightly during the mid-afternoon.

3.3. Mass scattering/extinction coefficients

For comprehensive analysis, we correlate hourly averages of b_{scat} and b_{ext} at 532 nm with aerosol mass concentration obtained in several ways. The first approach was to reconstruct PM_1 mass concentration by summing the AMS NR-PM_1 and EC measurements. As discussed above, this method may underestimate total PM_1 mass since some sea salt, metals, and mineral dusts are not included. The second approach was to sum $PM_{2.5}$ PILS anion data (chloride, sulfate, nitrate), with EC, and the AMS PM_1 ammonium and organic mass concentrations. This approach offers a higher size cut for anions, and the ability to sample ions present in sea salt. Finally, we used hourly $PM_{2.5}$ mass concentrations from the Burbank site (see above). This sampler was not co-located, but this method provides the most complete measurement of aerosol mass concentration. Results are shown in Fig. 4. Fig. 4A and B, illustrate that mass scattering and extinction coefficients were 4.9 and 5.1 $m^2\ g^{-1}$ when NR-PM_1 + EC data was used, with $R^2 = 0.8$. Fig. 4C–D show that mass scattering and extinction coefficients drop to 4.1 and 4.3 $m^2\ g^{-1}$ ($R^2 = 0.8$), respectively, due to higher

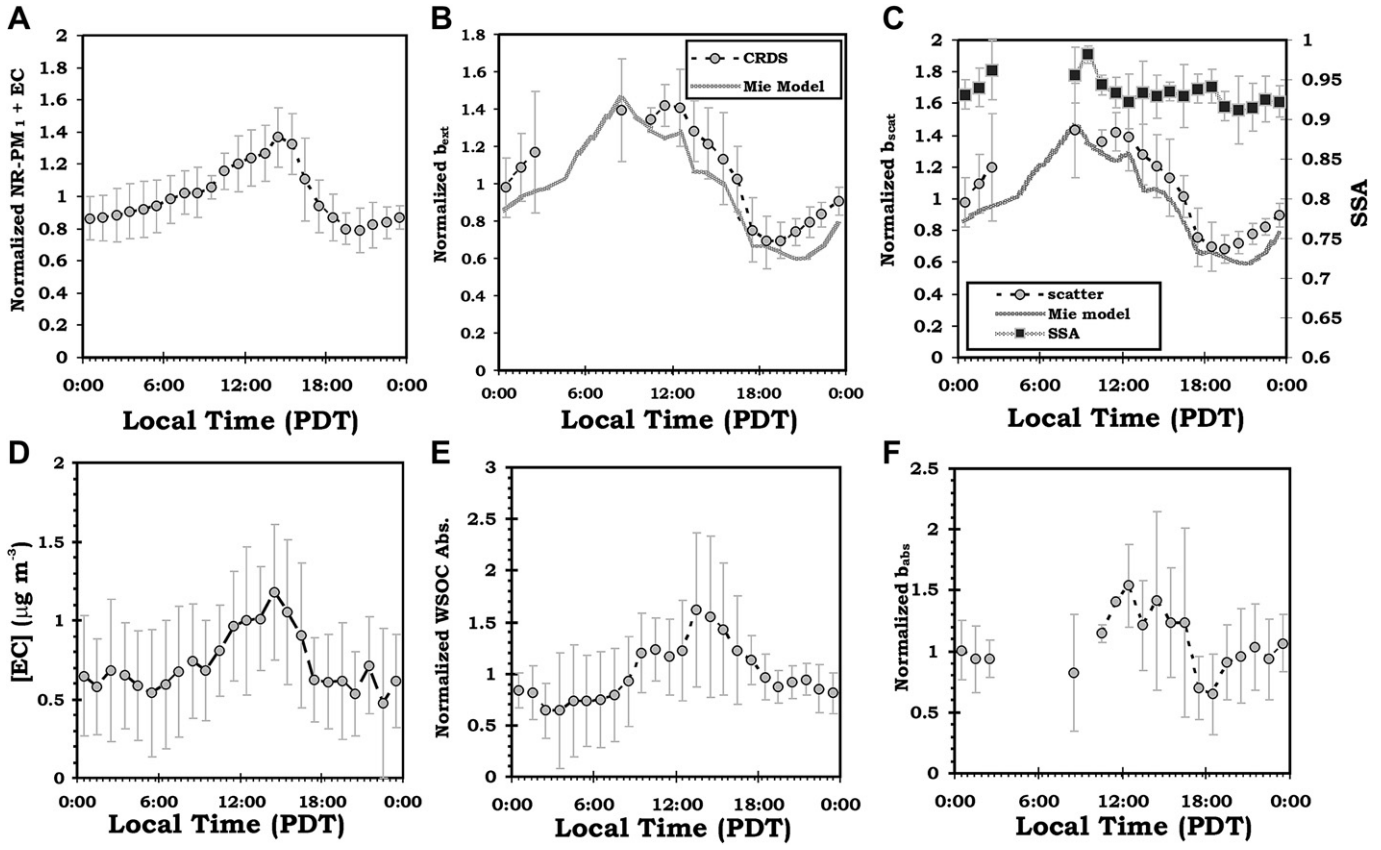

Fig. 3. Evaluation of diurnal patterns in (A) aerosol mass concentration, (B) b_{ext}, (C) b_{scat} and SSA, (D) EC mass concentration, (E) WSOC absorption at $\lambda = 365$ nm, and (F) b_{abs} at $\lambda = 532$ nm for the measurement period May 31–June 8 2010. All values except SSA and [EC] have been normalized to the observed daily mean to examine relative patterns. Hourly averages are reported and error bars are ±1 standard deviation. The missing albedometer data from the early morning hours arose because a persistent computer error prevented collection of optical data during this measurement time.

$PM_{2.5}$ mass concentrations when the PILS data is used for the anions. When the β-attenuation monitor measurements are used (Fig. 4E–F), mass scattering and extinction coefficients were 3.5 and 3.8 $m^2\ g^{-1}$, with a lower $R^2 = 0.5$, likely due to the distance between the sites. These trends are consistent with the expectations based on the additional sizes/species included in each version. The values for m_{scat} and m_{ext} reported for the CalNex measurement period are consistent with literature values in the range of 3–6 $m^2\ g^{-1}$ for urban areas (Ozkaynak et al., 1985; Waggoner et al., 1981).

3.4. Aerosol absorption, mixing state & mass absorption cross section (M.A.C.)

A plot of binned b_{abs} and EC mass concentrations (see Fig. 1D) yields a best-fit line with slope M.A.C. = 5.7 $m^2\ g^{-1}$. The lower and

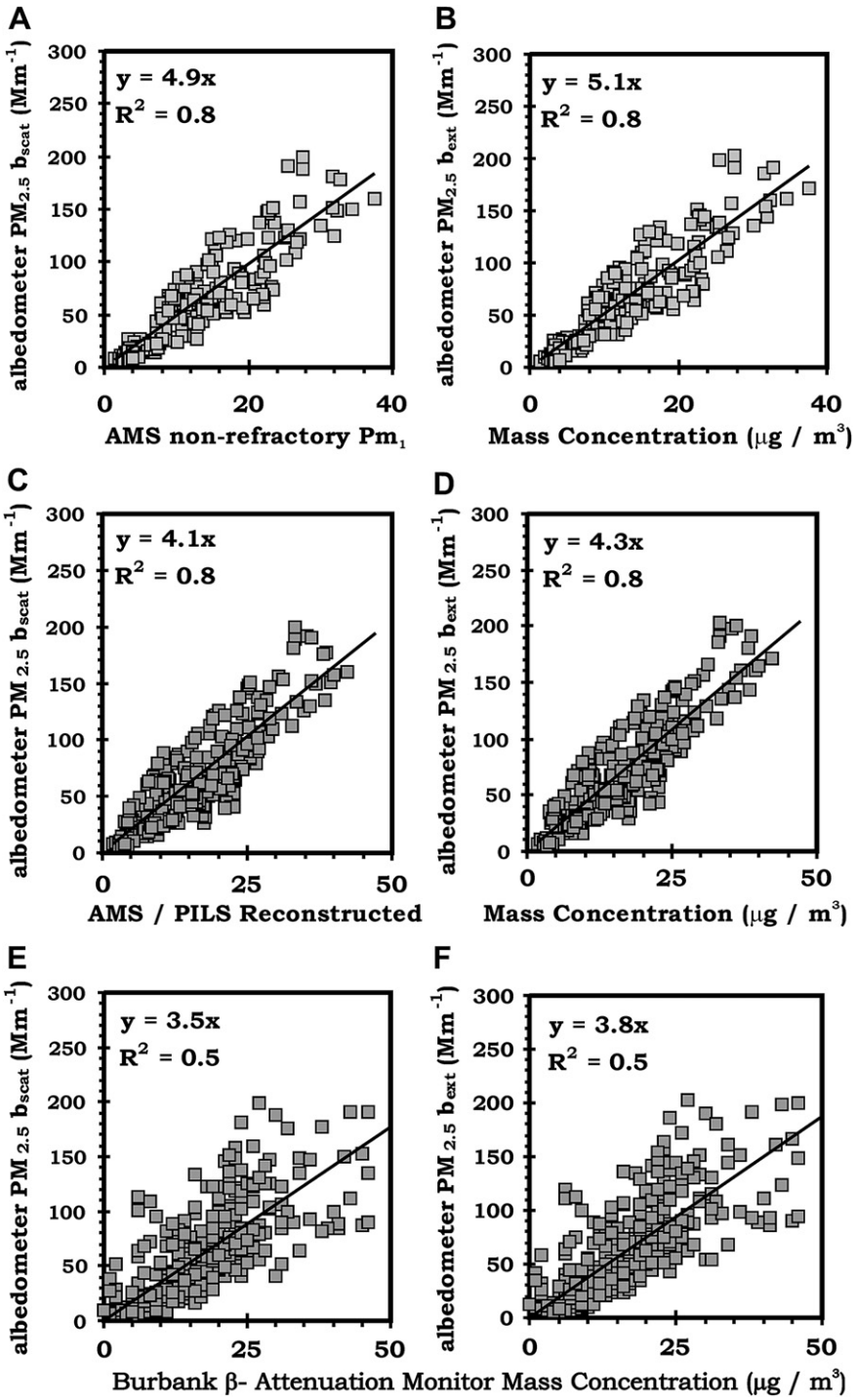

Fig. 4. Plots of observed aerosol b_{scat} and b_{ext} vs. aerosol mass concentration. Plots A and B are generated from AMS NR PM_1 mass concentration. Mass concentrations for plots C and D are reconstructed from PILS anion data and AMS organics/ammonium data for the Pasadena site. Plots E and F are generated using β -attenuation monitor data collected in Burbank. Scattering and extinction measured with aerosol albedometer with $PM_{2.5}$ inlet. All optical data collected at $\lambda = 532$ nm Slopes of the best-fit lines represent mass scattering and extinction efficiencies ($m^2\ g^{-1}$).

upper 95% confidence intervals for M.A.C. based on the fit were3.8 and 7.5 $m^2\ g^{-1}$, respectively. Signal averaging (binning) the hourly data resulted in good linearity between the variables ($R^2 = 0.95$), however, a scatter plot of hourly means was significantly more noisy. The mean value obtained for M.A.C. lies below the value Bond and Bergstrom (2006) suggest for fresh soot ($7.5 \pm 1.2\ m^2\ g^{-1}$). In addition, the result for M.A.C. is lower than values obtained from previous field studies. Liu et al. (2010) reported a median mass absorption cross section of $10.2 \pm 3.2\ m^2\ g^{-1}$ at $\lambda = 630$ nm for a European alpine site via use of a multi-angle absorption photometer (M.A.A.P.) and SP-2 (Droplet Measurement Technologies).Using an aethelometer and thermo-optical method, Jung et al. (2010) suggest an average mass absorption cross section of $9.4 \pm 1.8\ m^2\ g^{-1}$ at $\lambda = 550$ nm is appropriate for a site in Seoul, Korea. Yang et al. (2009) list a value of $9.5\ m^2\ g^{-1}$ for 550 nm for a site near Beijing (aethelometer + PSAP with thermo-optical method). Marley et al. (2009) report an average value of $7.7\ m^2\ g^{-1}$at 550 nm for two sites in and just outside of Mexico City (M.A.A.P. and aethelometer). However, the median values of Doran et al. (2007) extrapolated to 550 nm are between 12.8 and 14.3 $m^2\ g^{-1}$for suburban Mexico City sites (photoacoustic with thermo-optical). Andreae et al. (2008) report a value of $7.7\ m^2\ g^{-1}$for EC at 540 nm for a site near Guangzhou, China, which is very close to that postulated for fresh soot (also a photoacoustic with thermo-optical measurement). It is unclear the extent to which light absorbing organic matter affects these comparison data relative to the CALNEX data we report, but differences could certainly exist. Alternatively, methodological biases could be present.

Light scattering theory suggests when an absorbing core (e.g. soot) becomes coated/encapsulated by additional materials (secondary species) M.A.C. increases and absorption is enhanced because additional light is intercepted by the larger particle and focused onto the absorbing core. Bond et al. (2006) have suggested an increase in M.A.C. of approx. 1.5–2 fold is physically reasonable/plausible for a core-shell configuration; and results from laboratory studies suggest absorption enhancements of ~1–2 fold are possible for certain systems (Sedlacek et al., 2009; Schnaiter et al., 2005; Lack et al., 2009a, 2009b; Zhang et al., 2008; Shiraiwa et al., 2009; Schwarz et al., 2008). To investigate whether the CalNex data reflected such an effect, TEM images of particles collected at the Pasadena site were acquired to assess the morphology of soot particles, to study the extent to which they were coated, and to establish a quantitative index of the extent of soot coating.

Fig. 5A illustrates a TEM image of soot collected at the site. Soot was frequently internally mixed with sulfate and organics, and particles frequently demonstrated complex, irregular geometry. In urban environments, soot typically exists in internally mixed particles, with physical-chemical aging occurring within hours of emission at least in part through photochemical reaction and condensation of secondary materials (Adachi and Buseck, 2008). Fig. 5B illustrates the coated-soot fractions determined by TEM clearly increase with total NR-PM_1 mass concentrations (which are dominated by secondary species). This data suggests NR-PM_1 mass concentration is a useful metric to assess coatings on soot for Pasadena aerosol.

Soot particles were grouped as described in the methods section and M.A.C. values were compared with the TEM coating information. For this analysis, M.A.C. values are the mean hourly b_{abs} divided by corresponding EC mass concentration. Visual inspection of the trend (Fig. 6A) suggests the average M.A.C. value does not measurably change with coated-soot fraction. Fig. 6B and C illustrate plots of observed M.A.C. vs. NR-PM_1 or [NR-PM_1]/[EC]. Again, neither plot provides strong evidence for significant enhancement of light absorption due to soot coating as 95% confidence intervals overlap. To prepare Fig. 6B and C, all hourly average NR-PM_1 or [NR-PM_1]/[EC] values were ranked in ascending order and divided into 4 bins (quartiles) of equal number of data points. The hourly M.A.C. values and corresponding *x*- values for each bin were averaged and the resulting means were plotted. Visual inspection of TEM images (see for instance Fig. 5A) showed that sampled particles frequently do not have the ideal core-shell shape. Instead, soot is often found partially embedded in, or simply adhering to other materials. This result is consistent with the three-dimensional shapes of aerosol particles from Mexico City studied by TEM (Adachi et al., 2010), but may be inconsistent with the findings of other groups who have reported soot containing aerosols sampled in Riverside, CA are more consistent with a spherical geometry (Pratt and Prather, 2009; Moffet and Prather, 2009). While this analysis is useful for evaluating coatings on individual particles, the TEM method is affected by loss of semi volatile materials during sample preparation and analysis, and sample decomposition. It is well-known a significant fraction of aerosol is semi volatile (Pratt and Prather, 2009; Cappa and Jimenez, 2010; Huffman et al., 2009), so the evaporation of aerosol mass before or during TEM analysis likely represents a significant limitation. Additionally, this TEM analysis does not assess coating thickness, and the EC mass concentrations

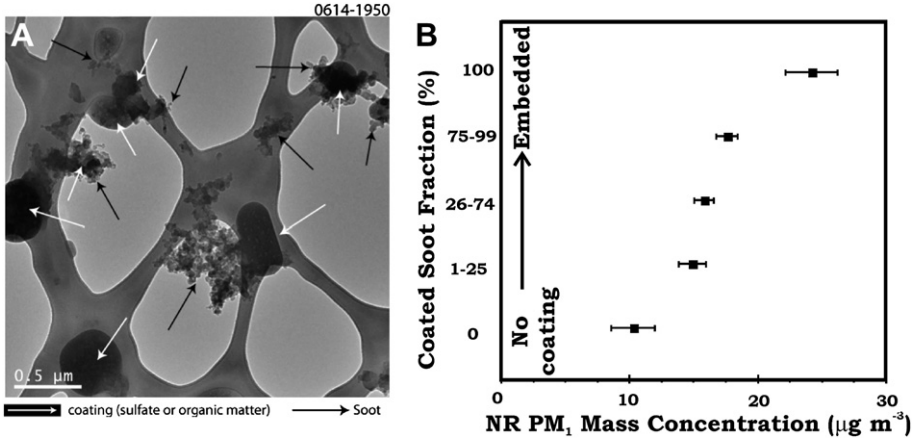

Fig. 5. (A) TEM image of internally mixed soot. Samples were collected on lacey-carbon TEM grids, which have carbon substrates that resemble the fibers of spider webs. Soot particles are partly or fully coated by organic matter, sulfate, or both. Coated soot particles generally do not have core-shell configuration when they are either coated or adhering to other aerosol particles. (B) The fraction of soot that is coated increases with NR-PM_1 concentration – this provides a useful metric of soot coating. Error bars represent standard errors.

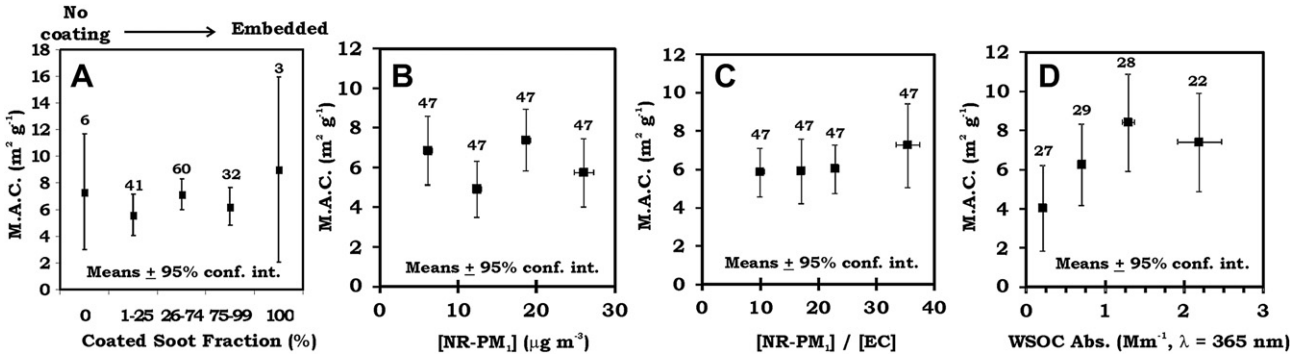

Fig. 6. (A) TEM analysis of coated-soot fractions (%) compared with apparent M.A.C. (B) Apparent M.A.C. plotted vs. NR-PM_1 mass concentration. (C) Apparent M.A.C. plotted vs. NR-PM_1 mass concentration normalized to EC mass concentration ([NR-PM_1]/[EC]). (D) Apparent M.A.C. vs. WSOC absorption. The number written above each data point represents the number of data points averaged in the bin. Error bars represent 95% confidence intervals computed for the bin. No trend in the data was detected for plots A–C given the measurement uncertainty and overlapping confidence intervals. However, as shown in plot D M.A.C. at 532 nm increased during periods of high WSOC light absorption.

are hourly means while the TEM analysis is conducted on a limited number of particles sampled over a few minutes during the same period as the EC measurement.

Several investigators have suggested various organic compounds in the aerosol may contribute to optical absorption (e.g. "brown carbon") (Gelencser et al., 2003; Shapiro et al., 2009; Chang and Thompson, 2010; Decesari et al., 2002; Adachi and Buseck, 2011; DeHaan et al., 2011). Certain nitrated organics are believed to be of particular importance to the LA basin (Jacobson, 1999). Simultaneous measurements of light absorption by water soluble organic carbon (WSOC) at the Pasadena site yielded a mean value of 0.71 $m^2\ g^{-1}$ C at $\lambda = 365$ nm with mean (stdev) absorption Ångstrom exponents of 3.2 (1.2) for the water soluble organic carbon (WSOC) component (Zhang et al., 2011). Extrapolation to 530 nm would yield values of $<0.25\ m^2\ g^{-1}$ C. Since the mass concentration of WSOC was typically $<4\ \mu g\ m^{-3}$ C for the campaign, the expected WSOC contribution to b_{abs} at 532 nm is $\leq 1\ Mm^{-1}$. This suggests absorption by soluble brown carbon contributes $\leq$25% to b_{abs} at 532 nm based on the campaign average b_{abs} of $\approx 4\ Mm^{-1}$. While this is a small magnitude of absorption, it may represent a significant fraction of total aerosol b_{abs} for LA. Fig. 6D illustrates the apparent effect of WSOC absorption on aerosol b_{abs}. The WSOC absorption data at $\lambda = 365$ nm (liquid phase measurement) was broken into quartiles and compared with simultaneously measured M.A.C. values. The resulting M.A.C. was found to nearly double during times of high WSOC absorption. This significant increase indicates that the presence of WSOC brown carbon may influence observations of aerosol b_{abs} and bias the M.A.C determined to falsely high values. Including all brown carbon (not just WSOC) could result in an even greater influence relative to EC. While this trend is apparent in the dataset, it is also very important to highlight caveats associated with the absorption data and the subsequent analysis presented in this work. Firstly, b_{abs} was generally small for the LA basin aerosol which adversely affects signal-to-noise. In addition, data from a photoacoustic spectrometer co-located at the site did not detect the influence of WSOC absorption on M.A.C. at 532 nm (J. Taylor, J. Allan, *personal communication*, 2010). The reason for the difference between the albedometer and photoacoustic data sets is not currently well-understood. Quantifying the exact visible absorption by the WSOC component in Pasadena requires additional supporting investigation.

4. Conclusion

An aerosol albedometer was used during CalNex 2010 to measure aerosol optical properties in the LA Basin. Mean $PM_{2.5}$ aerosol extinction, scattering, absorption coefficients, and single scattering albedo (b_{ext}, b_{scat}, b_{abs} and SSA) at $\lambda = 532$ nm were 62 Mm^{-1}, 58 Mm^{-1}, 4 Mm^{-1}, and 0.92, respectively. The aerosol optical densities were considerably lower than the historical record for this location, and aerosol absorption much lower than values encountered in other world megacities. Mass scattering and mass extinction coefficients of 3.5–5.1 $m^2\ g^{-1}$have been determined at a measurement wavelength of 532 nm. A campaign average mass absorption cross section (M.A.C.) of $5.7 \pm 1.8\ m^2\ g^{-1}$ is reported for EC. TEM analysis of sampled particles suggests soot is frequently mixed or adhering to other particles, but the particles often do not exhibit classic core-shell morphology. Alteration of M.A.C. with mixing/coating state was not detected, however, the presence of light absorbing, water-soluble organic carbon (WSOC) correlates with increases in M.A.C. measured via the albedometer and thermo-optical EC measurements.

Statement of author contributions

J. Thompson made albedometer optical measurements, conducted data analysis, reported results, and authored/edited the manuscript. P. Hayes and J. Jimenez provided AMS data, performed the Mie scattering reconstruction, and contributed significantly to authoring/editing the manuscript. K. Adachi and P. Buseck conducted the TEM analysis, reported coating ratio results, and assisted writing/editing the manuscript. X. Zhang, J. Liu, and R. Weber provided EC/OC mass concentration data, WSOC absorption data, PILS data, and contributed to authoring/editing the manuscript.

Acknowledgments

The authors thank Joost de Gouw, Jochen Stutz, Jason Surratt, John Seinfeld, and J.L. Jimenez, the organizers of the CalNex-LA effort, for their service to the community. We also thank Martin Graus and Joost de Gouw for providing the meteorological data presented. Caltech hosted the measurement site. P. Massoli and A. Freedman have provided aerosol extinction coefficients made via a cavity attenuated phase shift (CAPS) instrument for comparison. The entire CalNex community of scholars fostered a collaborative and stimulating environment during the campaign. The California Air Resources Board (CARB) and the National Oceanic & Atmospheric Administration (NOAA) provided funds to help establish the research site. We acknowledge the use of TEM facilities within the LeRoy Eyring Center for Solid State Science at Arizona State University. Special thanks to Kevin Durkee of South Coast Air Quality Management District for providing gravimetric PM data. The TEM study was supported by NSF grants ATM0531926 and

ATM1032312. K. A. acknowledges support from the global environment research fund of the Japanese Ministry of the Environment (A-1101). J.E.T.'s work has been funded in part by the State of Texas/Texas Tech University and in part by NSF grants ATM-0634872 and ATM-1004114. J.L.J. and P.L.H. acknowledge support from CARB 08-319 and DOE (BER/ASR Program) DE-SC0006035. P.L.H. acknowledges a CIRES visiting postdoctoral fellowship. R.J.W.'s work was funded through an NSF grant under contract number ATM-0931492.

Appendix. Supplementary material

Supplementary material associated with this article can be found, in the online version, at doi:10.1016/j.atmosenv.2012.03.011.

References

Adachi, K., Buseck, P.R., 2008. Internally mixed soot, sulfates, and organic matter in aerosol particles from Mexico City. Atmos. Chem. Phys. 8, 6469–6481. doi:10.5194/acp-8-6469-2008.

Adachi, K., Chung, S.H., Buseck, P.R., 2010. Shapes of soot aerosol particles and implications for their effects on climate. J. Geophys. Res. 115, D15206. doi:10.1029/2009JD012868.

Adachi, K., Buseck, P.R., 2011. Atmospheric tar balls from biomass burning in Mexico. J. Geophys. Res.-Atmos. 116, D05204. doi:10.1029/2010JD015102.

Adams, K.M., Davis, L.I., Japar, S.M., Finley, D.R., 1990. Real-time, in situ measurements of atmospheric optical absorption in the visible via photoacoustic spectroscopy – IV. Visibility degradation and aerosol optical properties in Los Angeles. Atmos. Environ. 24A (3), 605–610.

Aiken, A.C., Salcedo, D., Cubison, M.J., Huffman, J.A., DeCarlo, P.F., Ulbrich, I.M., Docherty, K.S., Sueper, D., Kimmel, J.R., Worsnop, D.R., Trimborn, A., Northway, M., Stone, E.A., Schauer, J.J., Volkamer, R., Fortner, E., de Foy, B., Wang, J., Laskin, A., Shutthanandan, V., Zheng, J., Zhang, R., Gaffney, J., Marley, N.A., Paredes-Miranda, G., Arnott, W.P., Molina, L.T., Sosa, G., Jimenez, J.L., 2009. Mexico city aerosol analysis during MILAGRO using high resolution aerosol mass spectrometry at the urban Supersite (T0). Part 1: fine particle composition and organic source apportionment. Atmos. Chem. Phys. 9, 6633–6653. doi:10.5194/acpd-9-8377-2009.

Andreae, M.O., Gelencsér, A., 2006. Black carbon or brown carbon? The nature of light-absorbing carbonaceous aerosols. Atmos. Chem. Phys. 6, 3131–3148. doi:10.5194/acp-6-3131-2006.

Andreae, M.O., Schmid, O., Yang, H., Chang, D., Yu, J.Z., Zeng, L.M., Zhang, Y.H., 2008. Optical properties and chemical composition of the atmospheric aerosol in urban Guangzhou, China. Atmos. Environ. 42 (25), 6335. doi:10.1016/j.atmosenv.2008.01.030.

Atkinson, R.W., Fuller, G.W., Anderson, H.R., Harrison, R.M., Armstrong, B., 2010. Urban ambient particle metrics and health: a time-series analysis. Epidemiology 21 (4), 501–511. doi:10.1097/EDE.0b013e3181debc88.

Bell, M.L., Belanger, K., Ebisu, K., Gent, J.F., Lee, H.J., Koutrakis, P., Leaderer, B.P., 2010. Prenatal exposure to fine particulate matter and birth weight: variations by particulate constituents and sources. Epidemiology 21 (6), 884–891. doi:10.1097/EDE.0b013e3181f2f405.

Birch, M.E., 1998. Analysis of carbonaceous aerosols: interlaboratory comparison. Analyst 123 (5), 851–857. doi:10.1039/a800028j.

Bond, T.C., Bergstrom, R.W., 2006. Light absorption by carbonaceous particles: an investigative review. Aerosol Sci. Technol. 40, 27–67.

Bond, T.C., Habib, G., Bergstrom, R.W., 2006. Limitations in the enhancement of visible light absorption due to mixing state. J. Geophys. Res. 111, D20211. doi:10.1029/2006JD007315.

Cappa, C.D., Jimenez, J.L., 2010. Quantitative estimates of the volatility of ambient organic aerosol. Atmos. Chem. Phys. 10, 5409–5424. doi:10.5194/acp-10-5409-2010.

California Air Resources Board (CARB), 2011. The Success of Air Pollution Controls in California (accessed 06.07.11.). http://www.arb.ca.gov/research/health/healthup/feb08.pdf.

Chang, J., Thompson, J.E., 2010. Characterization of colored products formed during irradiation of aqueous solutions containing H_2O_2 and phenolic compounds. Atmos. Environ. 44 (4), 541–551. doi:10.1016/j.atmosenv.2009.10.042.

Croes, B., 2011. Science to Improve California's Climate and Air Quality Programs. CALNEX Data Analysis Workshop, 16–19 May 2011, Sacramento, CA.

DeCarlo, P.F., Kimmel, J.R., Trimborn, A., Northway, M.J., Jayne, J.T., Aiken, A.C., Gonin, M., Fuhrer, K., Horvath, T., Docherty, K., Worsnop, D.R., Jimenez, J.L., 2006. Field-deployable, high-resolution, time-of-flight aerosol mass spectrometer. Anal. Chem. 78, 8281–8289. doi:10.1021/ac061249n.

Decesari, S., Facchini, M.C., Matta, E., Mircea, M., Fuzzi, S., Chugtai, A.R., 2002. Water soluble organic compounds formed by oxidation of soot. Atmos. Environ. 36 (11), 1827–1832. doi:10.1016/S1352-2310(02)00141-3.

DeHaan, D.O., Hawkins, L.N., Kononenko, J.A., Turley, J.J., Corrigan, A.L., Tolbert, M.A., Jimenez, J.L., 2011. Formation of nitrogen-containing oligomers by methylglyoxal and amines in simulated evaporating cloud droplets. Environ. Sci. Technol. 45 (3), 984–991. doi:10.1021/es102933x.

Dial, K.D., Hiemstra, S., Thompson, J.E., 2010. Simultaneous measurement of optical scattering and extinction on dispersed aerosol samples. Anal. Chem. 82 (19), 7885–7896. doi:10.1021/ac100617j.

Doran, J.C., Barnard, J.C., Arnott, W.P., Cary, R., Coulter, R., Fast, J.D., Kassianov, E.I., Kleinman, L., Laulainen, N.S., Martin, T., Paredes-Miranda, G., Pekour, M.S., Shaw, W.J., Smith, D.F., Springston, S.R., Yu, X.-Y., 2007. The T1-T2 study: evolution of aerosol properties downwind of Mexico city. Atmos. Chem. Phys. 7, 1585–1598. doi:10.5194/acp-7-1585-2007.

Eatough, D.J., Wadsworth, A., Eatough, D.A., Crawford, J.W., Hansen, L.D., Lewis, E.A., 1993. Multiple-system, multi-channel diffusion denuder sampler for the determination of fine-particulate organic material in the atmosphere. Atmos. Environ., Part A: General Topics 27A, 1213–1219.

Garland, R.M., Yang, H., Schmid, O., Rose, D., Nowak, A., Achtert, P., Wiedensohler, A., Takegawa, N., Kita, K., Miyazaki, Y., Kondo, Y., Hu, M., Shao, M., Zeng, L.M., Zhang, Y.H., Andreae, M.O., Pöschl, U., 2008. Aerosol optical properties in a rural environment near the mega-city Guangzhou, China: implications for regional air pollution, radiative forcing and remote sensing. Atmos. Chem. Phys. 8, 5161–5186. doi:10.5194/acp-8-5161-2008.

Gelencser, A., Hoffer, A., Kiss, G., Tombacz, E., Kurdi, R., Bencze, L., 2003. In-situ formation of light-absorbing organic matter in cloud water. J. Atmos. Chem. 45 (1), 25–33. doi:10.1023/A:1024060428172.

Hand, J.L., Day, D.E., McMeeking, G.M., Levin, E.J.T., Carrico, C.M., Kreidenweis, S.M., Malm, W.C., Laskin, A., Desyaterik, Y., 2010. Measured and modeled humidification factors of fresh smoke particles from biomass burning: role of inorganic constituents. Atmos. Chem. Phys. 10, 6179–6194. doi:10.5194/acp-10-6179-2010.

Haywood, J.M., Shine, K.P., 1995. The effect of anthropogenic sulfate and soot aerosol on the clear sky planetary radiation budget. Geophys. Res. Lett. 22 (5), 603–606.

Haywood, J., Boucher, O., 2000. Estimates of the direct and indirect radiative forcing due to tropospheric aerosols: a review. Rev. Geophys. 38 (4), 513–543. doi:10.1029/1999RG000078.

Hecobian, A., Zhang, X., Zheng, M., Frank, N., Edgerton, E.S., Weber, R.J., 2010. Water-soluble organic aerosol material and the light-absorption characteristics of aqueous extracts measured over the southeastern United States. Atmos. Chem. Phys. 10, 5965–5977. doi:10.5194/acp-10-5965-2010.

Huffman, J.A., Docherty, K.S., Mohr, C., Cubison, M.J., Ulbrich, I.M., Ziemann, P.J., Onasch, T.B., Jimenez, J.L., 2009. Chemically-Resolved volatility measurements of organic aerosol from different sources. Environ. Sci. Technol. 43, 5351–5357. doi:10.1021/es803539d.

I.P.C.C. – Climate Change, 2007. The Physical Science Basis. Working Group I Contribution to the Fourth Assessment Report of the Intergovernmental Panel on Climate Change (I.P.C.C.). Cambridge Press. 978 0521 70596–7.

Jacobson, M.Z., 1999. Isolating nitrated and aromatic aerosols and nitrated aromatic gases as sources of ultraviolet light absorption. J. Geophys. Res. 104, 3527–3542.

Jung, J., Kim, Y.J., Lee, K.Y., G.-Cayetano, M., Batmunkh, T., Koo, J.-H., Kim, J., 2010. Spectral optical properties of long-range transport Asian dust and pollution aerosols over Northeast Asia in 2007 and 2008. Atmos. Chem. Phys. 10, 5391–5408. doi:10.5194/acp-10-5391-2010.

Lack, D.A., Cappa, C.D., Cross, E.S., Massoli, P., Ahern, A.T., Davidovits, P., Onasch, T.B., 2009a. Absorption enhancement of coated absorbing aerosols: validation of the photo-acoustic technique for measuring the enhancement. Aerosol Sci. Technol. 43 (10), 1006–1012. doi:10.1080/02786820903117932.

Lack, D.A., Covert, D.C., Baynard, T., Massoli, P., Sieru, B., Lovejoy, E.R., Ravishankara, A.R., 2009b. Relative humidity dependence of light absorption by mineral dust after long-range atmospheric transport from the Sahara. Geophys. Res. Lett. 36, L24805. doi:10.1029/2009GL041002.

Liu, D., Flynn, M., Gysel, M., Targino, A., Crawford, I., Bower, K., Choularton, T., Jurányi, Z., Steinbacher, M., Hüglin, C., Curtius, J., Kampus, M., Petzold, A., Weingartner, E., Baltensperger, U., Coe, H., 2010. Single particle characterization of black carbon aerosols at a tropospheric alpine site in Switzerland. Atmos. Chem. Phys. 10, 7389–7407. doi:10.5194/acp-10-7389-2010.

Malm, W.C., Day, D.E., Kreidenweis, S.M., Collett Jr., J.L., Carrico, C., McMeeking, G., Lee, T., 2005. Hygroscopic properties of an organic laden aerosol. Atmos. Environ. 39 (27), 4969–4982. doi:10.1016/j.atmosenv.2005.05.014.

Marley, N.A., Gaffney, J.S., Castro, T., Salcido, A., Frederick, J., 2009. Measurements of aerosol absorption and scattering in the Mexico city metropolitan area during the MILAGRO field campaign: a comparison of results from the T0 and T1 sites. Atmos. Chem. Phys. 9, 189–206. doi:10.5194/acp-9-189-2009.

McMurry, P.H., Stolzenburg, M.R., 1989. On the sensitivity of particle size to relative humidity for Los Angeles aerosols. Atmos. Environ. 23 (2), 497–507. doi:10.1016/0004-6981(89)90593-3.

Moffet, R.C., Prather, K.A., 2009. In-situ measurements of the mixing state and optical properties of soot with implications for radiative forcing estimates. Proc. Natl. Acad. Sci. 106 (29), 11872–11877. doi:10.1073/pnas.0900040106.

Molina, L.T., Madronich, S., Gaffney, J.S., Apel, E., de Foy, B., Fast, J., Ferrare, R., Herndon, S., Jimenez, J.L., Lamb, B., Osornio-Vargas, A.R., Russell, P., Schauer, J.J., Stevens, P.S., Volkamer, R., Zavala, M., 2010. An overview of the MILAGRO 2006 Campaign: Mexico City emissions and their transport and transformation. Atmos. Chem. Phys. 10, 8697–8760. doi:10.5194/acp-10-8697-2010.

NIOSH, 1996. Elemental carbon (diesel particulate): method 5040. In: Eller, P.M., Cassinelli, M.E. (Eds.), NIOSH Manual of Analytical Methods. National Institute for Occupational Safety and Health, Cincinnati.

Orsini, D., Ma, Y., Sullivan, A., Sierau, B., Baumann, K., Weber, R., 2003. Refinements to the Particle-into-Liquid Sampler (PILS) for ground and airborne measurements of water soluble aerosol composition. Atmos. Environ. 37 (9–10), 1243–1259. doi:10.1016/S1352-2310(02)01015-4.

Ozkaynak, H., Schatz, A.D., Thurston, G.D., Isaacs, R.G., Husar, R.B., 1985. Relationships between aerosol extinction coefficients derived from airport visual range observations and alternative measure of airborne particle mass. J.A.P.C.A. 35, 1176–1185.

Paredes-Miranda, G., Arnott, W.P., Jimenez, J.L., Aiken, A.C., Gaffney, J.S., Marley, N.A., 2009. Primary and secondary contributions to aerosol light scattering and absorption in Mexico City during the MILAGRO 2006 campaign. Atmos. Chem. Phys. 9, 3721–3730. doi:10.5194/acp-9-3721-2009.

Pratt, K.A., Prather, K.A., 2009. Real-time, single-particle volatility, size, and chemical composition measurements of aged urban aerosols. Environ. Sci. Technol. 43, 8276–8282. doi:10.1021/es902002t.

Qian, F., December 2011. "Truncation Correction for the Aerosol Albedometer: Development and Laboratory Validation of Scattering Correction Factors." M.S. Thesis, Texas Tech University, Lubbock, TX.

Qian, F., Ma, L., Thompson, J.E., Angular truncation corrections for the aerosol albedometer: modeling and laboratory measurements of scattering correction factors. Measurement, submitted for publication.

Redmond, H., Dial, K., Thompson, J.E., 2010. Light scattering and absorption by wind blown dust: theory, measurement, and recent data. Aeolion Res. 2 (1), 5–26. doi:10.1016/j.aeolia.2009.09.002.

Redmond, H., Thompson, J.E., 2011. Evaluation of a Quantitative Structure Property Relationship (QSPR) for predicting mid-visible refractive index of secondary organic aerosol (SOA). Phys. Chem. Chem. Phys. 13, 6872–6882. doi:10.1039/C0CP02270E.

Schnaiter, M., Linke, C., Möhler, O., Naumann, K.-H., Saathoff, H., Wagner, R., Schurath, U., Wehner, B., 2005. Absorption amplification of black carbon internally mixed with secondary organic aerosol. J. Geophys. Res. 110, D19204. doi:10.1029/2005JD006046.

Schwarz, J.P., Spackman, J.R., Fahey, D.W., Gao, R.S., Lohmann, U., Stier, P., Watts, L.A., Thomson, D.S., Lack, D.A., Pfister, L., Mahoney, M.J., Baumgardner, D., Wilson, J.C., Reeves, J.M., 2008. Coatings and their enhancement of black carbon light absorption in the tropical atmosphere. J. Geophys. Res. 113, D03203. doi:10.1029/2007JD009042.

Shapiro, E.L., Szprengiel, J., Sareen, N., Jen, C.N., Giordano, M.R., McNeill, V.F., 2009. Light-absorbing secondary organic material formed by glyoxal in aqueous aerosol mimics. Atmos. Chem. Phys. 9, 2289–2300. doi:10.5194/acp-9-2289-2009.

Shiraiwa, M., Kondo, Y., Iwamoto, T., Kita, K., 2009. Amplification of light absorption of black carbon by organic coating. Aerosol Sci. Technol. 44 (1), 46–54. doi:10.1080/02786820903357686.

Sedlacek, A.J., Lee, J., Onasch, T.B., Davidovits, P., Cross, E.S., 2009. Light Absorption by Coated Soot. American Geophysical Union. Fall Meeting 2009, abstract #A13C-0239.

Sueper, D., June 2011. ToF-AMS Analysis Software. Available online at: http://cires.colorado.edu/jimenez-group/wiki/index.php/ToF-AMS_Analysis_Software.

Sullivan, A.P., Weber, R.J., Clements, A.L., Turner, J.R., Bae, M.S., Schauer, J.J., 2004. A method for on-line measurement of water-soluble organic carbon in ambient aerosol particles: results from an urban site. Geophys. Res. Lett. 31, L13105. doi:10.1029/2004GL019681.

Thompson, J.E., Barta, N., Policarpio, D., DuVall, R., 2008. A fixed frequency aerosol albedometer. Opt. Express 16, 2191–2205. doi:10.1364/OE.16.002191.

Waggoner, A.P., Weiss, R.E., Ahlquist, N.C., 1981. Optical characteristics of atmospheric aerosols. Atmos. Environ. 15, 1891–1909.

Yan, P., Pan, X., Tang, J., Zhou, X., Zhang, R., Zeng, L., 2009. Hygroscopic growth of aerosol scattering coefficient: a comparative analysis between urban and suburban sites at winter in Beijing. Particuology 7 (1), 52–60. doi:10.1016/j.partic.2008.11.009.

Yang, M., Howell, S.G., Zhuang, J., Huebert, B.J., 2009. Attribution of aerosol light absorption to black carbon, brown carbon, and dust in China – interpretations of atmospheric measurements during EAST-AIRE. Atmos. Chem. Phys. 9, 2035–2050. doi:10.5194/acp-9-2035-2009.

Zadoo, S., Thompson, J.E., 2011. Rayleigh scattering measurements of several fluorocarbon gases. J. Environ. Monit. 13 (11), 3294–3297.

Zhang, R., Khalizov, A.F., Pagels, J., Zhang, D., Xue, H., McMurry, P.H., 2008. Variability in morphology, hygroscopicity, and optical properties of soot aerosols during atmospheric processing. Proc. Nat. Acad. Sci. 105, 10291–10296. doi:10.1073/pnas.0804860105.

Zhang, X., Lin, Y.-H., Surratt, J.D., Zotter, P., Prevot, A.S.H., Weber, R.J., 2011. Light-absorbing soluble organic aerosol in Los Angeles and Atlanta: a contrast in secondary organic aerosol. Geophys. Res. Lett. 38, L21810. doi:10.1029/2011GL049385.